AMERICAN SOCIETY FOR MICROBIOLOGY | Microbiology Spectrum

RESEARCH ARTICLE

GpsB Coordinates Cell Division and Cell Surface Decoration by Wall Teichoic Acids in *Staphylococcus aureus*

Lauren R. Hammond,[a] Michael D. Sacco,[b] Sebastian J. Khan,[a] Catherine Spanoudis,[a] Abigail Hough-Neidig,[a] Yu Chen,[b] Prahathees J. Eswara[a]

[a]Department of Cell Biology, Microbiology, and Molecular Biology, University of South Florida, Tampa, Florida, USA
[b]Department of Molecular Medicine, University of South Florida, Tampa, Florida, USA

Lauren R. Hammond and Michael D. Sacco contributed equally to this article. Author order was determined by the seniority of involvement in this project.

ABSTRACT Bacterial cell division is a complex and highly regulated process requiring the coordination of many different proteins. Despite substantial work in model organisms, our understanding of the systems regulating cell division in noncanonical organisms, including critical human pathogens, is far from complete. One such organism is *Staphylococcus aureus*, a spherical bacterium that lacks known cell division regulatory proteins. Recent studies on GpsB, a protein conserved within the *Firmicutes* phylum, have provided insight into cell division regulation in *S. aureus* and other related organisms. It has been revealed that GpsB coordinates cell division and cell wall synthesis in multiple species. In *S. aureus*, we have previously shown that GpsB directly regulates FtsZ polymerization. In this study, using *Bacillus subtilis* as a tool, we isolated spontaneous suppressors that abrogate the lethality of *S. aureus* GpsB overproduction in *B. subtilis*. Through characterization, we identified several residues important for the function of GpsB. Furthermore, we discovered an additional role for GpsB in wall teichoic acid (WTA) biosynthesis in *S. aureus*. Specifically, we show that GpsB directly interacts with the WTA export protein TarG. We also identified a region in GpsB that is crucial for this interaction. Analysis of TarG localization in *S. aureus* suggests that WTA machinery is part of the divisome complex. Taken together, this research illustrates how GpsB performs an essential function in *S. aureus* by directly linking the tightly regulated cell cycle processes of cell division and WTA-mediated cell surface decoration.

IMPORTANCE Cytokinesis in bacteria involves an intricate orchestration of several key cell division proteins and other factors involved in building a robust cell envelope. Presence of teichoic acids is a signature characteristic of the Gram-positive cell wall. By characterizing the role of *Staphylococcus aureus* GpsB, an essential cell division protein in this organism, we have uncovered an additional role for GpsB in wall teichoic acid (WTA) biosynthesis. We show that GpsB directly interacts with TarG of the WTA export complex. We also show that this function of GpsB may be conserved in other GpsB homologs as GpsB and the WTA exporter complex follow similar localization patterns. It has been suggested that WTA acts as a molecular signal to control the activity of autolytic enzymes, especially during the separation of conjoined daughter cells. Thus, our results reveal that GpsB, in addition to playing a role in cell division, may also help coordinate WTA biogenesis.

KEYWORDS WTA, FtsZ, GpsB, suppressors, cell division, cell wall, cytokinesis, PBP

One of the defining characteristics of life is the ability for a cell to grow and divide. Although there are some exceptions, the predominant process for growth and division in bacteria is binary fission where one bacterial cell grows and divides to produce two similarly sized daughter cells (1–4). Although significant strides have been made to identify the molecular mechanism regulating the cell division machinery, gaps remain in our knowledge,

Editor M.-N. Frances Yap, Northwestern University

Address correspondence to Prahathees J. Eswara, eswara@usf.edu.

The authors declare no conflict of interest.

Received 26 April 2022
Accepted 12 May 2022
Published 1 June 2022

particularly in the nonmodel organisms (2, 5). For example, GpsB (the central protein of interest in this study) plays an important, and in some cases essential, role in the cell growth regulation of multiple clinically relevant Gram-positive organisms (specifically *Firmicutes*) but is absent in Gram-negative organisms (6, 7). This highlights the need for a closer analysis of such processes and proteins in multiple species.

In *Bacillus subtilis*, *Listeria monocytogenes*, and *Streptococcus pneumoniae*, GpsB links cell wall biosynthesis with the cell division process by interacting with penicillin-binding proteins (PBPs), thereby helping to regulate and maintain proper cell shapes (8–14). Our lab reported that *Staphylococcus aureus* GpsB directly interacts with FtsZ and affects its polymerization characteristics (15). In our previous study, we described the lethal phenotype associated with the overproduction of *S. aureus* GpsB ($GpsB^{SA}$) in its *Firmicutes* relative *B. subtilis*. In this study, we utilized this phenotype to conduct a suppressor screen to identify residues that are important for the function of $GpsB^{SA}$ and pathways through which $GpsB^{SA}$ may exert its function. Herein, we describe the effects of seven intragenic $GpsB^{SA}$ suppressor mutations and characterize their ability to abrogate cell division inhibition. Additionally, we investigated extragenic suppressor mutations through whole-genome sequencing that allowed us to delineate a novel role for GpsB in linking central cell division directly to the wall teichoic acids (WTA) pathway. Specifically, suppressor mutations were mapped to *tagG/tagH* genes in *B. subtilis*, and subsequent bacterial two-hybrid (BACTH) analysis confirmed the direct interaction between $GpsB^{SA}$ and the *S. aureus* homolog of TagG, TarG. We also show a 3-amino-acid motif, positioned away from the well-characterized PBP-binding site, that appears to be important for TarG binding. Furthermore, we show that the interaction between GpsB and the WTA export complex may be conserved beyond *S. aureus*, as we also note that TagH has a spatiotemporal localization pattern similar to that of GpsB in *B. subtilis* cells. In *S. aureus*, treatment with antibiotics that target the WTA pathway drastically alters the localization pattern of GpsB, although targeting of GpsB to new division sites remains unaffected. Thus, it appears that GpsB, an essential protein in *S. aureus*, coordinates cell division and WTA production/transport through direct interaction with FtsZ and TarG, respectively.

RESULTS

Isolation of suppressor mutations of $GpsB^{SA}$ overproduction in *B. subtilis*. Previously, we showed that overexpression of $gpsB^{SA}$ leads to cell death in *B. subtilis* (15) in a manner independent of native GpsB or other known/possible interaction partners of *B. subtilis* GpsB such as PBP1, EzrA, PrkC, and DivIVA (7). We also noticed that *B. subtilis* cells appear filamentous due to impaired FtsZ ring assembly in the presence of excess $GpsB^{SA}$. In that report, we demonstrated that the role of $GpsB^{SA}$ is to regulate the polymerization kinetics of FtsZ in *S. aureus*. To build upon our previous report and further explore other cell cycle processes that involve $GpsB^{SA}$ in an unbiased manner, we isolated suppressors that can tolerate the lethal overproduction of $GpsB^{SA}$ in *B. subtilis* (15). Briefly, a *B. subtilis* strain harboring an isopropyl-β-D-thiogalactopyranoside (IPTG)-inducible $gpsB^{SA}$-*gfp* was streaked out on plates containing IPTG and incubated overnight. Following incubation, the colonies that appeared on the plates containing the inducer were presumed to contain spontaneous suppressor mutations. Non-green-fluorescent-protein (GFP)-producing isolates were discarded, as the likely cause of the suppression of lethality could be a promoter mutation turning off the expression of $gpsB^{SA}$-*gfp*, a frameshift mutation, or a premature truncation. After multiple rounds of confirmatory screening, the mutations were classified to be either intragenic or extragenic (Fig. 1A) (16). Using this method, we isolated seven intragenic mutations, Y14F, L35S, D41N, D41G, and R72H as well as a deletion and repeat of a 3-amino-acid stretch, 66 to 68 LEE (ΔLEE and LEErpt), that are listed in Fig. 1B; of these, L35S was reported previously (15). Throughout this article, these suppressor mutations as a group will be referred to as *GpsB-GFP. We then analyzed the multiple sequence alignment of GpsB from *S. aureus*, *B. subtilis*, *L. monocytogenes*, and *S. pneumoniae* (Fig. 1C). Of the first four mutations (Y14F, L35S, D41N, and D41G), the latter three occur in highly conserved residues. Tyr14 is wedged between a conserved Lys (Lys11) which was reported to be important for forming a bidentate salt bridge with the proximal glutamate/aspartate (Glu15 in *S. aureus*) in other organisms (6). Of

A

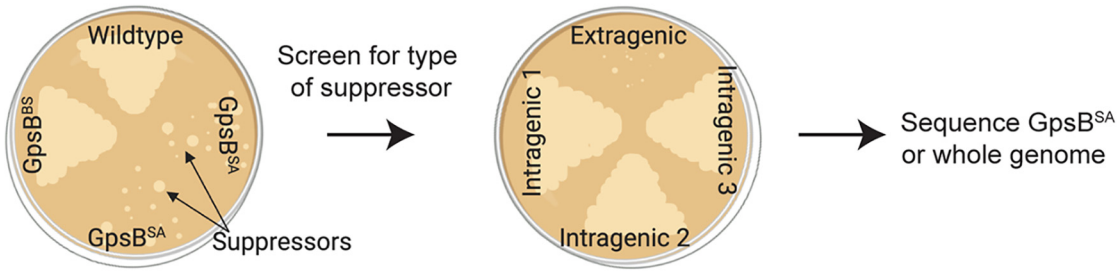

B

Suppressor #	*Mutation*	*Amino Acid Change*	*Position*
1	TAT to TTT	Y14F	14
2	TTA to TCA	L35S	35
3	GAT to GGT	D41G	41
4	GAT to AAT	D41N	41
5	(TTAGAAGAA) deletion	ΔLEE	66-68
6	(TTAGAAGAA) repeat	LEErpt	66-68
7	CGT to CAT	R72H	72

C

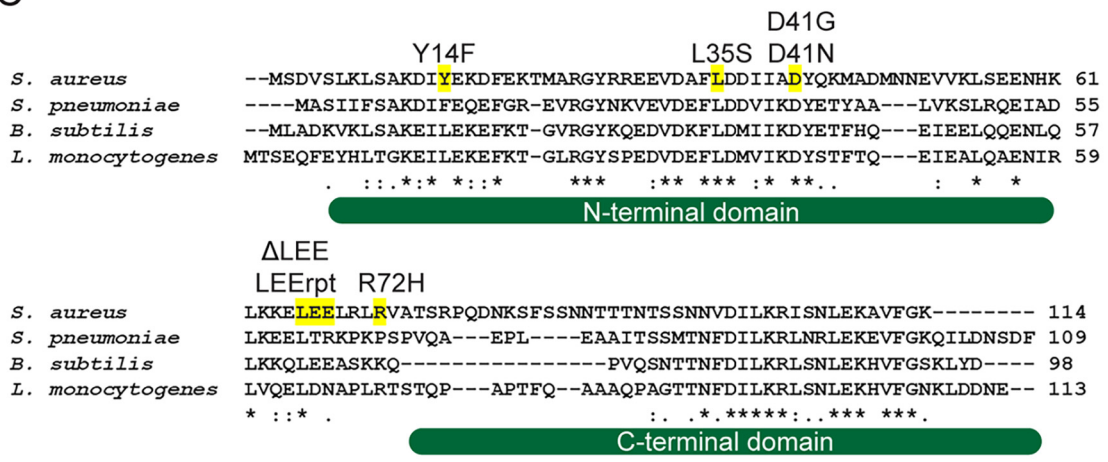

FIG 1 GpsB^{SA}-GFP suppressor screen. (A) Cartoon diagram depicting workflow for GpsB^{SA}-GFP suppressor screen (16). Figure generated using Biorender.com. (B) Table describing seven isolated GpsB^{SA}-GFP intragenic suppressor mutations detailing the mutation, amino acid change, and amino acid position. (C) Multiple sequence alignment of GpsB from *S. aureus*, *S. pneumoniae*, *B. subtilis*, and *L. monocytogenes*. Intragenic suppressor mutations identified in the GpsB^{SA}-GFP suppressor screen are highlighted in yellow and labeled above the residue locations. *, :, and . indicate fully, strongly, or weakly conserved residues, respectively. The structured N- and C-terminal domains are shown under the sequence alignment as reported previously (6).

note, Phe replaces Tyr in the corresponding position (Tyr14 of *S. aureus*) in *S. pneumoniae* GpsB. The remaining three mutations (ΔLEE, LEErpt, and R72H) are near the disordered linker connecting the N- and C-terminal domains (Fig. 1C). The Leu, Glu, and Glu (LEE) motif is conserved in *B. subtilis*; however, Arg72 is less conserved but appears in *L. monocytogenes*.

Suppressor mutations of GpsB^{SA} abolish cell division inhibition in *B. subtilis* cells. To examine the ability of *B. subtilis* to tolerate the expression of **gpsB^{SA}-gfp*, we conducted a spot titer assay with a clean copy of *gpsB^{SA}-gfp* harboring the suppressor mutation cloned into PY79 cells under the control of an inducible promoter, similar to how the wild-type *gpsB^{SA}-gfp* was constructed. Cultures containing each of the strains were grown, serially diluted, and then plated onto LB agar plates both with and without the inducer

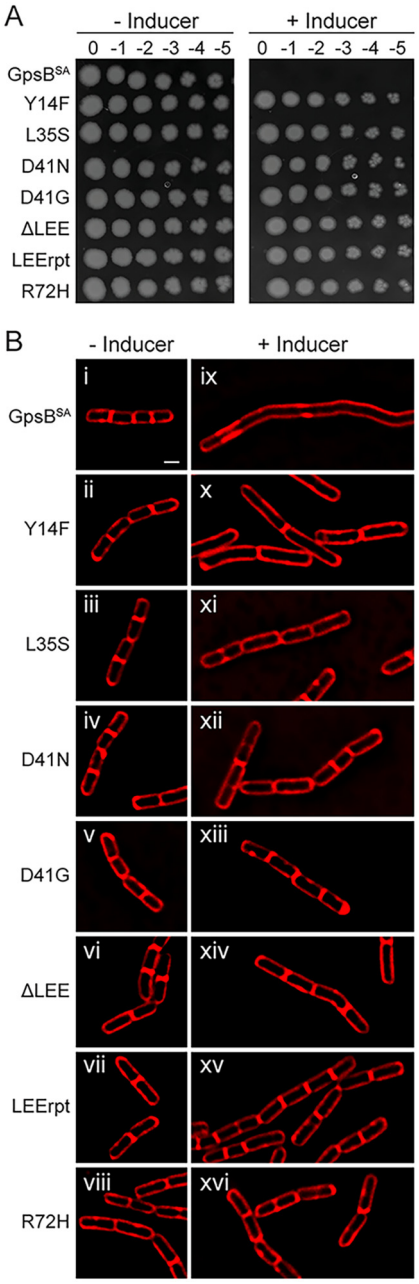

FIG 2 Growth characteristics of intragenic suppressor mutations of GpsB^{SA}-GFP. (A) Spot titer assay of unmutated GpsB^{SA}-GFP (GG8; top row) and isolated *GpsB^{SA}-GFP intragenic suppressor mutations (CS89 to CS93, PE377, and PE448) were serially diluted, spotted on plates, and grown in the absence (left panel) or presence (right panel) of 1 mM IPTG. (B) Cell morphology of cells harboring unmutated GpsB^{SA}-GFP (GG8) and the *GpsB^{SA}-GFP intragenic suppressor mutations (CS89-CS93, PE377, and PE448) grown in the absence (i to viii) or presence (ix to xvi) of 1 mM IPTG. Images were taken 3 h after addition of inducer. Membrane was stained with SynaptoRed membrane dye. Scale bar is 1 μm.

(Fig. 2A). On the minus inducer plate, all strains were able to grow and no growth defects were noted. On the plus inducer plate, the strain containing unmutated GpsB^{SA}-GFP showed a severe growth defect consistent with our previous report. In contrast, the growth on the minus inducer plates and that on the plus inducer plates for each of the suppressor mutations were indistinguishable from each other. Western blotting was used to confirm the stable production of each mutant in *B. subtilis* (Fig. S1A). Although most suppressors are stably produced, L35S displayed a distinct cleavage product (Fig. S1B) and LEErpt appears to be more stable, as it accumulates to a larger extent even in the absence of the inducer.

Regardless, all seven suppressor mutations in GpsB^{SA} allow *B. subtilis* cells to grow on solid medium in the presence of inducer.

We previously reported that the growth defect caused by the expression of *gpsB*^{SA} in *B. subtilis* was due to severe filamentation, which is characteristic of cell division inhibition in this organism (15). To investigate the effect of the suppressor mutations on cell division inhibition, we performed high-resolution fluorescence microscopy (Fig. 2B). Upon expression of *gpsB*^{SA}*-gfp*, we observed the previously reported cell division inhibition and filamentous phenotype (Fig. 2B, panel ix). Notably, upon expression of each of the suppressor mutations, the *B. subtilis* cells no longer display the filamentous phenotype and appear to be dividing normally (Fig. 2B, panels x to xvi). We also examined *GpsB-GFP localization in all strains (Fig. S1C). Diffused localization was observed for the L35S (as noted previously; see reference 15) and D41N suppressors (Fig. S1C, panels iii and v). Otherwise, all *GpsB-GFP strains displayed either division site localization (LEErpt and R72H) or foci similar to WT-GpsB^{SA}.

Most **gpsB*^{SA} mutants are dominant alleles and can suppress the toxicity of *gpsB*^{SA} upon coexpression. To determine if any of the **gpsB* mutations suppress the toxicity of the wild-type *gpsB*^{SA} allele, we engineered a *B. subtilis* strain to coexpress both *gpsB*^{SA}*-gfp* and **gpsB*^{SA}*-gfp* under the control of an IPTG-inducible promoter to produce stoichiometrically equivalent amounts of both wild-type and mutant proteins. We then performed a spot titer assay to examine any growth defects in these strains (Fig. S2A). In the strains carrying the suppressor mutations, six were able to restore growth and grow both in the absence and in the presence of inducer. The seventh mutation, Y14F, showed a weak dominant negative effect as it was able to grow in serial dilutions 2 to 3 log-fold higher than GpsB^{SA}-GFP alone. However, it was not as strong as the other mutations that grew in a serial dilution that was 5 to 6 log-fold higher than GpsB^{SA}-GFP. Interestingly, cells overproducing Y14F variants were on average longer (3.92 μm, $n = 100$) than the minus inducer control (2.18 μm, $n = 100$), implying partial functionality of this mutant (compare Fig. 2B, panels ii and x). Next, we used a BACTH assay to examine the protein-protein interactions that could explain this dominant negative effect. Since GpsB is known to form a hexamer (trimer of dimers), we tested the ability of each mutant to interact with WT-GpsB^{SA} by cloning GpsB^{SA} and *GpsB^{SA} into the BACTH plasmids (17). Pairs of these plasmids were transformed into BTH101 *Escherichia coli* cells for protein-protein interaction analysis on MacConkey agar and by β-galactosidase assay in liquid cultures (Fig. S2B). We found that all the mutants retained their ability to interact with WT GpsB. Thus, we believe that a GpsB^{SA}-*GpsB^{SA} interaction is likely the reason for the suppression in toxicity observed in Fig. S2A.

As GpsB is an essential protein in *S. aureus*, we wondered if the expression of these dominant suppressor mutation-harboring copies of *gpsB* would impair the essential function of GpsB^{SA} in its native organism and be lethal to the cells. This straightforward analysis was complicated by the fact that overproduction of *gpsB-gfp* in *S. aureus* by itself is toxic and results in cell enlargement as reported previously (15). Thus, we were not able to conduct a thorough analysis. However, among these suppressors, it appears that Y14F, ΔLEE, and R72H are the most potent in inhibiting the function of native GpsB, as colony formation is almost completely eliminated upon their overproduction (Fig. S2C). Stable production of *GpsB^{SA}-GFP in *S. aureus* cells was also confirmed through Western blotting (Fig. S2D). Despite being one of the most toxic mutations, the ΔLEE mutant accumulates to a much lower extent than the other mutants.

Structural modeling analysis of GpsB^{SA} suppressor mutations. The N-terminal domain of GpsB is characterized by an elongated coiled-coil dimer that is highly conserved among homologs (Fig. 3 and Fig. S3) and is highly similar to the lipid-binding domain of DivIVA (6). The GpsB monomer has two regions of organized secondary structure: a long α-helix of approximately 35 to 40 residues (α-helix 2) and a shorter, two-turn α-helix of approximately 8 residues (α-helix 1) (Fig. 3A). Near the membrane-binding region, α-helix 1 from one protomer converges at the interface of α-helix 2 and α-helix 1 from the other protomer to form a groove that binds to the cytoplasmic N-terminal domain of PBPs (6, 7). Although the PBP-binding site is conserved among GpsB homologs, a conclusive positive interaction between *S. aureus* GpsB and any of the PBPs has not been observed yet. The N-terminal domain of GpsB is connected by a nonconserved, disordered linker to a short, helical C-terminal domain.

Using the SWISS-MODEL homology-server, a homology model for the N terminus of *S. aureus* GpsB was constructed, allowing us to predict the structural effects of these

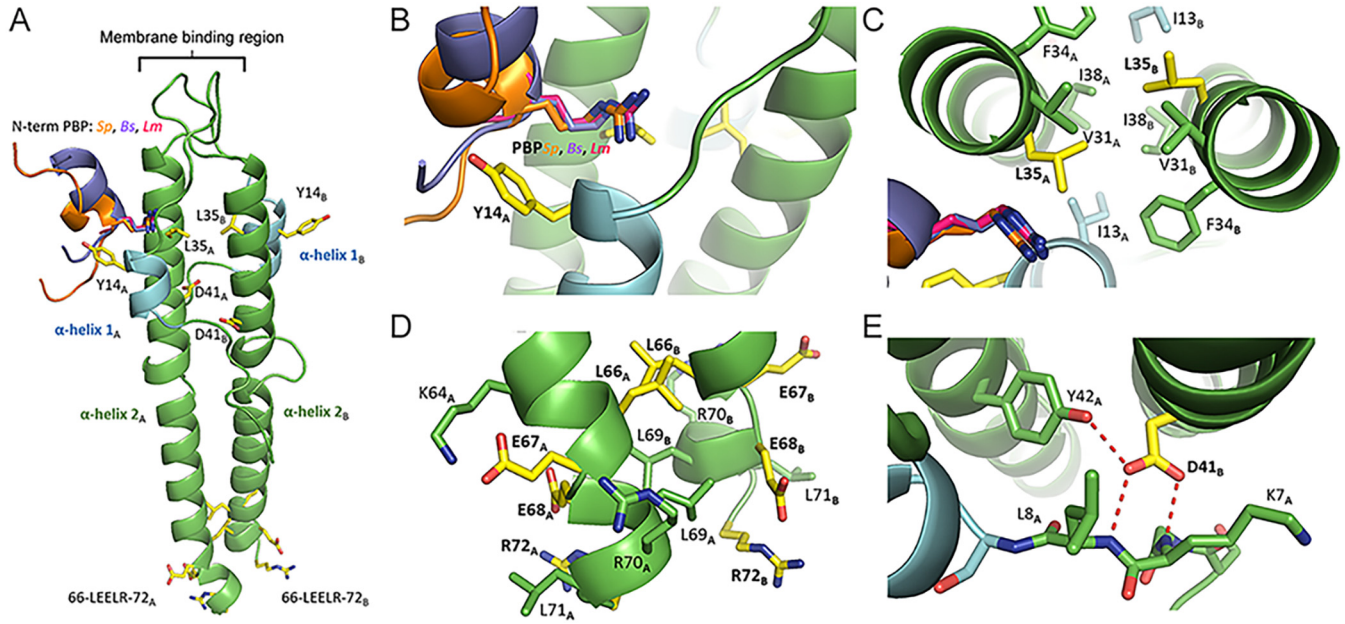

FIG 3 Homology model of *S. aureus* GpsB. Residues mutated in the experiments are colored in yellow. The 8 residues of α-helix 2 S9-E15 are colored in blue. (A) The N-terminal domains of *S. pneumonia* PBP2a (PDB ID 6GQN, orange), *B. subtilis* PBP1a (PDB ID 6GP7, lavender), and *L. monocytogenes* PBPA1 (PDB ID 6GPZ, magenta) bound to GpsB were superimposed and are shown to illustrate the highly conserved PBP-binding groove. (B) The Y14F mutation occurs on α-helix 1 and points directly toward the putative PBP-binding partner. (C) The L35S mutation occurs at the junction of the hydrophobic, coiled-coiled core of α-helices $2_{A,B}$ and the PBP-binding groove. (D) The D41N and D41G mutations occur at the interface of the loop formed by the first 8 residues and the two adjacent helices of α-helix 2 from protomers A and B. (E) The LEELR sequence is the last of α-helix 2 before it transitions into a disordered linker sequence that bridges the N-terminal domain to the C-terminal domain.

suppressor mutations (Fig. 3) (18). The mutations described in our experiments likely disrupt the structural integrity of GpsB (L35S, D41N/D41G) or alter the recognition elements required for partner binding (Y14F, R72H, LEE repeat/deletion).

(i) Tyr14 → Phe. Tyr14 is located on α-helix 1 near the PBP-binding groove where it is oriented outwards, away from the core and into the solvent accessible region (Fig. 3B). The aliphatic nature of the Tyr side chain is conserved in *S. pneumoniae*, *L. monocytogenes*, and *B. subtilis* where it is Phe, Leu, and Leu, respectively. Using the structures of *L. monocytogenes*, *B. subtilis*, and *S. pneumoniae* GpsB complexed with their PBP-binding partners (PDB IDs 6GPZ, 6GP7, and 6GQN, respectively), we observe that Tyr14 projects directly toward the PBP N-terminal helix (10, 14). Because Tyr14 does not interact with other residues in GpsB and the Tyr → Phe mutation is relatively minor, a likely scenario for the more toxic phenotype (Fig. S2C) is that Tyr14 facilitates interaction with a binding partner. Furthermore, because the Tyr → Phe mutation corresponds to the loss of a phenolic hydroxyl group, the interaction likely involves the formation of a hydrogen bond.

(ii) Leu35 → Ser. Leu35 is positioned at the interface of the PBP-binding site and the core of the coiled-coil junction (Fig. 3C). Despite interacting with adjacent hydrophobic residues near the interfacial core, Leu35 is in immediate proximity to the canonical arginine that is required for PBP binding. However, a mutation to a more polar residue that is capable of hydrogen bonding would seemingly improve this interaction. Therefore, it is most likely that the L35S mutation disrupts the core hydrophobic interactions that are critical for maintaining either the overall structure or the shape of the PBP-binding groove. This may explain the diffused localization (Fig. S1). Further supporting this hypothesis is an equivalent mutation at this position in *L. monocytogenes* GpsB, L36A, that prevents oligomerization of GpsB, presumably due to the disruption of this hydrophobic core (10).

(iii) Asp41 → Asn, Gly. Asp41 is located on α-helix 2 where it interacts with a loop formed by the first 10 residues of GpsB that precedes α-helix 1 (Fig. 3E and Fig. S3C). Given the proximity of Asp41 to Lys7 and the fact that a mutation to the chemically similar but neutral Asn produces a nonfunctional variant, one could mistakenly assume this is a critical electrostatic interaction. However, the side chain of Lys7 is 5.8 Å away from the closest Asp side

chain oxygen, well beyond the expected range of favorable electrostatic interactions. Furthermore, Lys7 is not conserved among *L. monocytogenes* and *S. pneumoniae*; significantly, *S. pneumoniae* GpsB has an isoleucine at this position (Fig. S3C). A closer inspection of this region reveals that Asp41 is an important acceptor of three hydrogen bonds from the strictly conserved Tyr42 of the adjacent protomer and the amide nitrogen of the Lys7 and Leu8 main chain. The hydrogen bonds with the backbone nitrogen of Lys7 and Leu8 are important interactions because this attracts the loop to the helical core of GpsB, allowing α-helix 1 to interact with α-helix 2, thus correctly forming the PBP-binding groove. Therefore, the replacement of any of the Asp oxygen atoms, even with a nitrogen hydrogen bond donor, would likely prohibit the formation of these three highly coordinated hydrogen bonds.

(iv) LEE deletion/repeat and Arg72 → His. The last two turns of the GpsB N-terminal α-helix 2 are composed of residues 66-LEELRLR-72. They are followed by a flexible linker region of approximately 20 amino acids that connects to the C-terminal domain. Interestingly, the LEELRLR region is not conserved among other *Firmicutes* and is unique to *S. aureus*. Multiple i +3 and i +4 electrostatic interactions are formed laterally along LEELRLR by Arg and Glu sidechains and Lys64 (Fig. 3D and Fig. S4). Additionally, the Leu residues interact through hydrophobic interactions in the core with the corresponding residue of the adjacent protomer and the neighboring Leu of its own chain. The insertion or deletion of a LEE sequence would disrupt the complementarity of sidechain interactions and cause charge-charge repulsion. Deletion of LEE eliminates a pair of (N + 3/N + 4) +/− interactions (K64-E67, E68) and (E68-R72) while adding one pair of +/+ interactions (K63, K64-E67R) (Fig. S4C). A LEE repeat eliminates one +/− interaction (E68-R72) and adds two pairs of −/− interactions: (E67-R70E, L71E) and (E68-L71E, R72E) (Fig. S4B). Therefore, the insertion or deletion of LEE will decrease the helical propensity of this region. Because the disruption of secondary structure is restricted to a small region that is adjacent to a disordered linker, the impact on the overall structure of GpsB structure could be minimal, meaning this specific area may have functional importance for binding to other proteins. Possible proteins include FtsZ (15) or other unique interaction partners (such as TarG discussed later in this report) that could interact with GpsB through LEELRLR. Additionally, Arg72 is either the last residue of α-helix 2 or the beginning of the disordered linker region that connects the N-terminal domain to the C-terminal domain. Either way, it is unlikely to affect the overall structure of GpsB and could also be a critical residue that interacts with another protein, likely through electrostatic interactions with a Glu or Asp residue.

Isolation of extragenic suppressors reveals a link between GpsB and wall teichoic acid machinery. In addition to the intragenic suppressors described above, we also isolated extragenic suppressors and then analyzed these mutants through whole-genome sequencing (Fig. 1A). Through this process, we isolated three different suppressor mutations independently. Two of the mutants had the same mutation in *tagH* (Y233C), and the third suppressor had a mutation in *tagG* (R20K) (Fig. 4A and Fig. S6). TagG and TagH work together to form a complex that exports WTA that are made intracellularly so they can be anchored to the cell wall (19). As these WTA genes are essential in *B. subtilis*, to confirm that the extragenic suppressors harbor true suppressor mutations we utilized the previously developed essential gene knockdown tool based on CRISPR interference (CRISPRi) with deactivated Cas9 (20) to disrupt the expression of either *tagG* or *tagH*. Briefly, we investigated the fate of wild-type GpsB^{SA}-GFP-overproducing cells when *tagG* or *tagH* expression was knocked down (+ xylose) or not (Fig. 4C). When we imaged these *tagG* or *tagH* strains without xylose (Fig. 4B, panels i and iii), the strains appeared similar to the wild type. Upon addition of xylose, we noted areas of membrane enrichment near cell poles (Fig. 4B, panels ii and iv), consistent with the previous report of bulging (20). As shown before (Fig. 2B), induction of *gpsB^{SA}-gfp* expression with IPTG leads to filamentation (Fig. 4C, panels i and ii). In the CRISPRi strains of *tagG* or *tagH* with GpsB^{SA}-GFP, the IPTG-mediated filamentation is also seen in the absence of xylose (no interference in the expression of *tagG* or *tagH*) (Fig. 4C, panels iv and viii). Finally, when we added both IPTG and xylose to induce GpsB^{SA}-GFP production and knockdown of *tagG* or *tagH*, the cells were no longer filamentous (Fig. 4C, panels vi and x), thus confirming that *tagG* and *tagH* are true suppressors of GpsB^{SA}-GFP-mediated cell division inhibition. Therefore, it is likely that the extragenic suppressor mutations result in dysregulation of the TagGH complex to suppress

A

Suppressor #	*Gene*	*Mutation*	*Amino Acid Change*
1	*tagH*	TAC to TGC	Y233C
2	*tagH*	TAC to TGC	Y233C
3	*tagG*	AGA to AAA	R20K

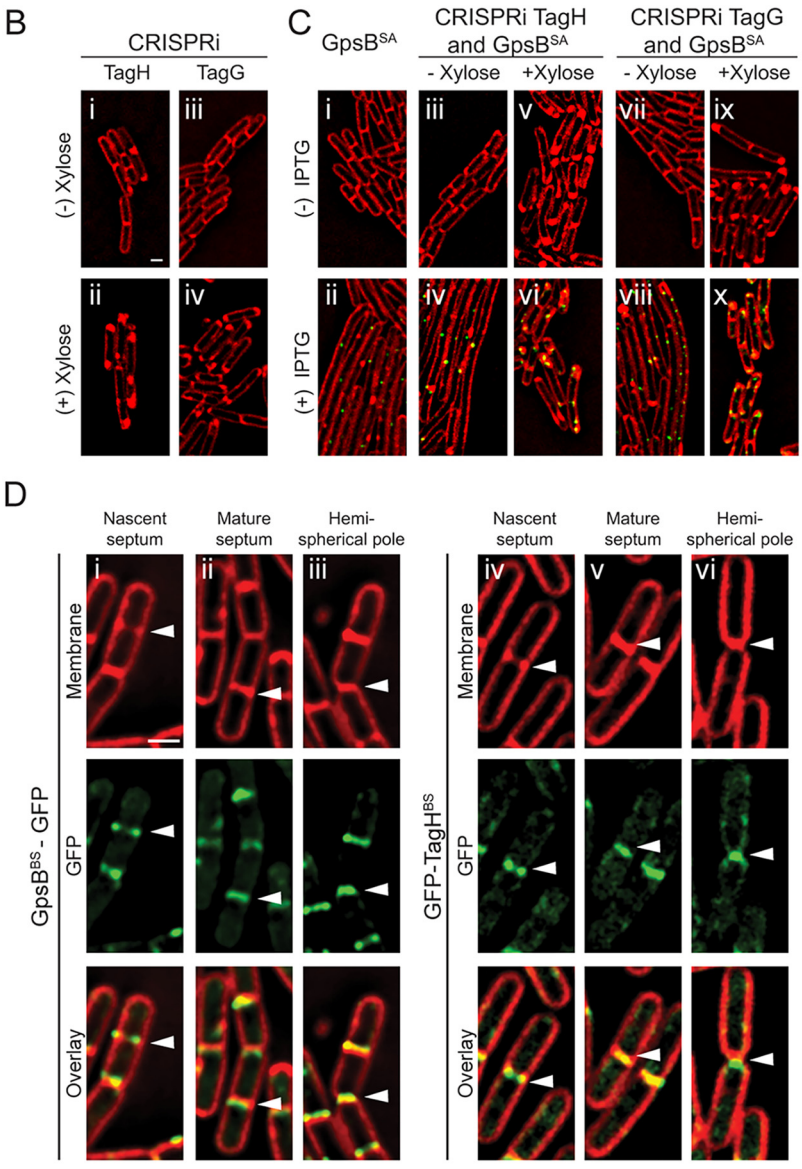

FIG 4 Analysis of GpsB^{SA}-GFP extragenic suppressor mutations. (A) Table describing the three isolated extragenic suppressor mutations detailing the specified gene, mutation, and amino acid change. (B) Fluorescence microscopy showing the cell morphology of strains containing a CRISPRi knockdown of *tagH* (SK16) and *tagG* (SK15) in *B. subtilis* grown in the absence (i and iii) and presence (ii and iv) of 1% xylose. (C) Cells containing inducible *gpsB*^{SA}*-gfp* (GG8) grown in the absence (i) and presence (ii) of 1 mM IPTG. Strains constructed to have both the CRISPRi knockdown of either *tagH* or *tagG* as well as inducible *gpsB*^{SA}*-gfp* (SK18 and SK17) were imaged in the absence of xylose and IPTG (iii and vii), in the presence of xylose only (v and ix), in the presence IPTG only (iv and viii), and finally in the presence of both xylose and IPTG (vi and x). Cells imaged 3 h after the addition of xylose and/or IPTG. Scale bar is 1 μm. (D) Fluorescence micrographs tracking the localization pattern of GpsB^{BS}-GFP (GG19; i to iii) and GFP-TagH^{BS} (PE528; iv to vi) through different stages of the cell division (see arrowheads). Cell membrane is visualized with SynaptoRed membrane dye. Scale bar is 1 μm.

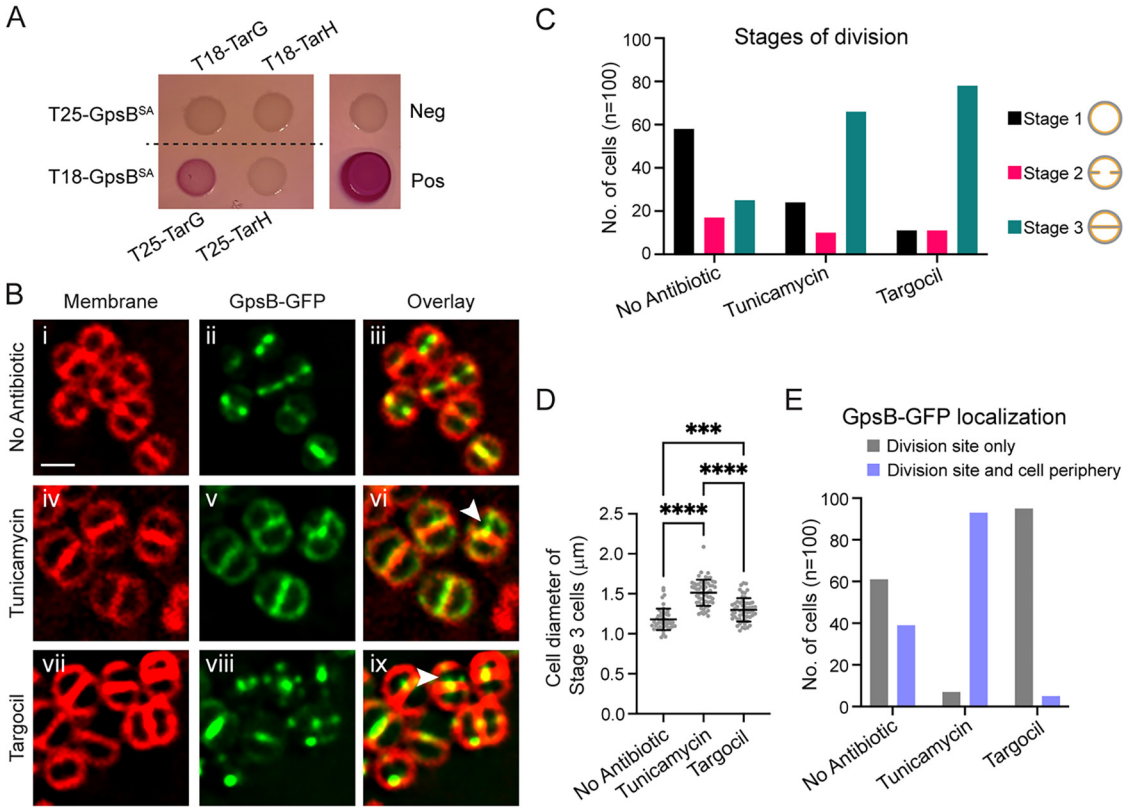

FIG 5 Characterization of the link between WTA exporter TarGH and GpsB in *S. aureus*. (A) Bacterial two-hybrid assay to investigate pairwise interactions of GpsB^{SA} with *S. aureus* TarG (SKB1 and SKB2) and TarH (SKB3 and SKB4). A color change to deep pink indicates a positive interaction. Images taken after 24 h of incubation. (B) Localization pattern of GpsB^{SA}-GFP (PES6) in SH1000 *S. aureus* cells following 1 h of treatment with 20 μg/mL tunicamycin (iv to vi) or 8 μg/mL targocil (vii to ix). White arrowheads show instances of GpsB^{SA}-GFP localizing to the next division site despite incomplete cell separation. Cell membranes visualized with SynaptoRed membrane dye. Scale bar is 1 μm. (C) Number of cells in each stage of division following 1 h of treatment with tunicamycin or targocil. Stage 1 (black bars) cells show no membrane enrichment at midcell. Stage 2 cells (pink bars) have some membrane enrichment at midcell but do not have fully formed septa. Stage 3 (teal bars) are cells that have fully formed septa at midcell. (D) Quantification of cell diameters from stage 3 cells treated with tunicamycin or targocil; n = 100 cells; ***, P = 0.0002; ****, $P < 0.0001$. One-way analysis of variance (ANOVA) and multiple comparisons performed in GraphPad Prism 9. (E) Number of stage 3 cells showing localization of GpsB-GFP at the division site only (gray) or at the division site and the periphery (purple) following 1 h of treatment of tunicamycin or targocil; n = 100 cells.

the lethal overexpression of *gpsB*^{SA}. Perhaps the reduced function of TagGH allows cell division to proceed by freeing up the components required for PG synthesis (such as lipid-II).

To our knowledge, a direct relationship of GpsB and WTA synthesis has not been reported in *B. subtilis*. So, to investigate how TagGH could suppress GpsB^{SA}-GFP-mediated cell division inhibition, we monitored both GpsB and TagGH localization in *B. subtilis* cells. Using GpsB^{BS}-GFP and GFP-TagH^{BS} (21), we analyzed when TagH arrived at the division site (Fig. 4D). We found that both GpsB^{BS} and TagH^{BS} arrive at midcell early in the division cycle (at a similar time to GpsB^{SA} in *B. subtilis* [15]) in areas of membrane enrichment (indicating the regions of septal membrane invagination) (Fig. 4D, panels i and iv, see arrowhead) and stays at the mature septum (Fig. 4D, panels ii and v), at least until the septum transforms into hemispherical cell poles (Fig. 4D, panels iii and vi). This is consistent with the previous reports of TagH^{BS} (21) and GpsB^{BS} localization (8, 9). Thus, it appears that GpsB may play a role in WTA biosynthesis by interacting with one or more of the WTA biosynthesis proteins, and the toxicity stemming from GpsB^{SA} production in *B. subtilis* could be due to an interaction between GpsB^{SA} and the TagGH^{BS} WTA exporter complex.

GpsB^{SA} directly interacts with *S. aureus* wall teichoic acid export protein TarG. Next, we analyzed whether GpsB^{SA} could interact directly with the *S. aureus* homolog of TagGH, TarGH (Tag, teichoic acid glycerol; Tar, teichoic acid ribitol) (19) using a BACTH assay. We detected a strong positive interaction between TarG^{SA} and GpsB^{SA} both on solid medium (Fig. 5A) and by quantifying the production of β-galactosidase enzyme in liquid culture

(Fig. S5A). To further confirm that GpsB^{SA} and TarG^{SA} interact in *S. aureus* cells, we performed a coimmunoprecipitation assay using FLAG-tagged GpsB as a bait. We detected GFP-TarG in the eluate but not SigA, which served as our negative control (Fig. S5B). This indicates that the TarG/GpsB interaction is physiologically relevant in *S. aureus*. Interestingly, a previous work showed an interaction between GpsB^{SA} and TarO^{SA} via BACTH (22).

Since we could detect an interaction between GpsB and the WTA export complex, and given that a knockdown of TagGH rescues GpsB^{SA}-mediated filamentation in *B. subtilis*, we were curious if overexpression of *gpsB^{SA}* would lead to reduced WTA levels in *S. aureus* cells. To test this hypothesis, purified crude WTA extracts from *S. aureus* cells containing either an empty vector or one overproducing GpsB were visualized under Alcian blue silver staining, but we did not detect any changes in WTA levels in these cells at the condition tested (Fig. S5C). Since GpsB^{SA} is essential, we were not able to test the effect of GpsB depletion on WTA levels due to pleiotropic effects stemming from the role of GpsB in cell division (15). Thus, it is unclear whether GpsB is directly able to modulate the WTA export function of TarGH complex.

To further investigate the relationship between GpsB and TarG, we studied the localization pattern of GFP-TarG and observed that TarG localizes to the division site at the onset of membrane invagination (Fig. S5D). This supports the physiological significance of GpsB-TarG interaction, as GpsB also localizes to nascent division sites (Fig. 5B) (15). These data suggest that GpsB is perhaps involved in the localization of TarGH to the division site. In support of this model, division site localization of the WTA biosynthesis protein TarO (TagO) has also been noted in *S. aureus* (23). The division site localization of TarO and TarG and their direct interaction between GpsB reveal that WTA machinery may be part of the divisome complex in *S. aureus*.

GpsB regulation of FtsZ is independent of wall teichoic acid synthesis. Our previous report showed that GpsB interacts with FtsZ and localizes to the site of division in *S. aureus*, so we wanted to see if GpsB localization at midcell was dependent on ongoing wall teichoic acid synthesis/export (Fig. 5B). For this purpose, we used two inhibitors of wall teichoic acid synthesis, tunicamycin (early WTA biosynthesis by TarO is inhibited [24]), and targocil (TarGH-mediated WTA export is inhibited [25]). It is noteworthy that in addition to targeting TarO, tunicamycin could also target the early-stage peptidoglycan biosynthesis protein MraY at higher concentration (24). Based on previous observations, treatment with these antibiotics does not halt cell division; however, the placement of the septa and overall regulation of division are disrupted. Treated cells also had significant cell separation defects presumably due to limited autolysin activity (24–28). Given this information, we used high-resolution fluorescence microscopy to monitor the localization of GpsB^{SA}-GFP in cells treated with tunicamycin or targocil. *S. aureus* cells containing GpsB^{SA}-GFP were grown to mid-log, and then the inducer (IPTG) and the antibiotics (tunicamycin or targocil) were added and cells were grown for an additional hour. At this point, the majority of cells were expected to have completed a full round of division in our experimental condition. In the cultures treated with either tunicamycin or targocil, cells were significantly larger (Fig. 5B and D). The impaired autolytic activity is also evident, with 25% of cells having a completed septum designated "stage 3" in the no-antibiotic-treatment control versus 66% in the tunicamycin-treated cells and 78% in the targocil-treated cells (Fig. 5C). Despite the impaired cell separation in both the tunicamycin- and targocil-treated cells, we noted evidence of GpsB localizing to sites perpendicular to the previous plane of division (Fig. 5B, panels vi and ix, white arrowheads), suggesting that although the cells are not separating properly, they are still attempting to undergo another round of division and that GpsB and presumably FtsZ localization/regulation remain intact. Interestingly, we did note one distinct phenotype between the tunicamycin- and targocil-treated cells. In the cells treated with tunicamycin, GpsB-GFP appears to remain localized in the peripheral membrane in addition to sites of division; however, in the targocil-treated cells, there is very little peripheral membrane localization (Fig. 5B, panels v and viii, and Fig. 5E).

Intragenic mutants reveal critical residues for GpsB/TarG interaction. The homology modeling of our intragenic GpsB mutants revealed that three of the mutations, ΔLEE, LEErpt, and R72H, could disrupt protein-protein interactions. To investigate whether any of

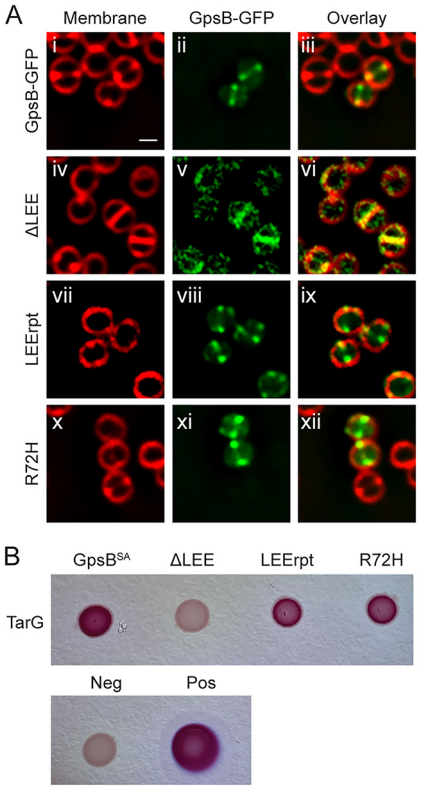

FIG 6 Characterizing GpsB residues important for TarG interaction. (A) Localization pattern of GpsB-GFP (GGS2) or *GpsB-GFP (ΔLEE, LEErpt, R72H; LH17, LH35, LH18) in RN4220 *S. aureus* cells. Cells imaged 1 h after the addition of 1 mM IPTG and stained with SynaptoRed membrane dye. Scale bar is 1 μm. (B) Bacterial two-hybrid assay of pairwise interactions of TarG (SKB2) and GpsB (LH39) or *GpsB (ΔLEE, LEErpt, R72H; LH47, LH43, LH55). A color change to deep pink indicates a positive interaction. Images were taken after 24 h of incubation.

these three mutations affected their localization, we imaged these strains under fluorescence microscopy. As longer incubation with ΔLEE and R72H is lethal (Fig. S2C), cells were imaged at an earlier time point (1 h postinduction). We noted that all three mutations, ΔLEE, LEErpt, and R72H, retained wild-type-like localization (Fig. 6A). Next, we tested the ability of these mutants to interact with TarG. Using the BACTH assay, we tested the interactions of ΔLEE, LEErpt, and R72H with TarG. We observed that LEErpt and R72H were still able to interact with TarG; however, ΔLEE no longer interacted with TarG (Fig. 6B). We further ensured adenylate cyclase-tagged ΔLEE is stably produced (Fig. S5F). These data suggest that the presence of these three residues (or the length of the disordered linker connecting the N- and C-terminal domains) is important for the GpsB-TarG interaction. As such, it is tempting to speculate whether the lethality of dominant ΔLEE overproduction (Fig. S2C) could be due to the impairment of the native GpsB and TarG interaction.

It has been reported that targocil treatment (inhibition of WTA export) could prevent the translocation of major autolysin, Atl (28). It was shown that *S. aureus* cells treated with targocil exhibited reduced autolysis compared to that of untreated cells. We were interested in testing whether GpsB promoted or inhibited WTA export-mediated autolysis (Fig. S5E). The rate of autolysis did not change significantly between cells harboring an inducible copy of *gpsB*, *gpsB*$^{\Delta LEE}$, and the empty vector (EV) control. However, as reported previously, subsequent to targocil treatment, the strain harboring EV control displayed reduced autolysis. Interestingly, in targocil-treated cells overproducing GpsB, the autolysis was reproducibly higher than that in the EV control. This increased autolysis is dependent on TarG interaction, as overproduction of ΔLEE (which lacks the interaction with TarG; Fig. 6B) mimicked EV control. Thus, it appears that GpsB may facilitate autolysin (Atl) translocation through its interaction with the TarG component of the WTA export machinery.

DISCUSSION

GpsB is highly conserved across the *Firmicutes* phylum. In *B. subtilis*, *S. pneumoniae*, and *L. monocytogenes*, GpsB is involved in the coordination of cell division and cell wall synthesis through the binding of PBPs and other partners (6, 7, 14). Our lab recently reported a novel function of *S. aureus* GpsB in regulating FtsZ polymerization by promoting lateral interactions and facilitating GTP hydrolysis (15). In this study, we characterized several different mutations in $GpsB^{SA}$ in an effort to more thoroughly understand GpsB-mediated cell division regulation in *S. aureus*. Subsequent to a suppressor screen, we identified TarG as a protein interaction partner of GpsB in *S. aureus* and found that residues 66 to 68 (LEE) of GpsB are critical for this interaction. An earlier BACTH investigation of *S. aureus* cell division factors and peptidoglycan synthesis machinery identified an interaction between EzrA and GpsB; however, it failed to show an interaction between GpsB and any other proteins, including PBPs (PBP1, PBP2, and PBP3) (29). However, it appears that GpsB may interact with PBP4 (22), which plays a role in peripheral peptidoglycan synthesis in *S. aureus* (30). An extensive BACTH-based interaction analysis between lipoteichoic acid (LTA) biosynthesis proteins and cell division factors also revealed that GpsB is not part of the LTA complex in *S. aureus* (31). Thus, our finding of TarG-GpsB interaction is insightful and was only suspected based on our unbiased approach. In addition to the GpsB interaction with TarG shown here, previous work showed that GpsB interacts with TarO in *S. aureus* (among other proteins) (22).

Traditionally, WTA export has been alluded to occur along the lateral cell wall with the possible help of shape-determining MreB, MreC, and/or MreD proteins in *B. subtilis* (21, 32–34), which could allow for higher order accumulation of WTA at the lateral cell wall. Consistent with this model, several WTA biosynthesis proteins, including TagGH, also interact with FtsEX, which is involved in cell elongation in *B. subtilis* (35, 36). However, evidence suggests that WTA synthesis is not only important for cell elongation, as a role for FtsEX in cell division and cell separation has been elucidated in *S. pneumoniae* (37) (and it is also known that FtsEX can directly interact with FtsZ in the Gram-negative organism *Escherichia coli* [38]). A role for FtsEX in the activation of a specific peptidoglycan hydrolase has been well documented in these organisms (36–39). Additionally, of the proteins discussed above, MreC is a known interaction partner of GpsB in *B. subtilis*, *S. pneumoniae*, and *L. monocytogenes* (8, 14). Interestingly, MreC and other GpsB interaction partners, PBP1 and EzrA, also interact with FtsEX in *B. subtilis* (35). Thus, it is possible to envision a complex made of Mre proteins, FtsEX, PBPs, and GpsB moderating the WTA biosynthesis in *B. subtilis*. Although well-studied MreB is absent in *S. aureus*, MreC and MreD proteins are present and are targeted to the division sites (40), similar to GpsB (15). Surprisingly, *S. aureus* lacks the genes for FtsE and FtsX (L. Aravind, National Center for Biotechnology Information/National Institutes of Health, personal communication). During the course of evolution into a spherical organism from a rod-shaped ancestor, it appears that *S. aureus* has lost the need for the FtsEX complex. However, another alternate mechanism(s) to activate cell wall hydrolases, such as LytH/ActH (41), exists. Thus, it is possible that in *S. aureus* the WTA machinery is positioned and regulated differently than its nonspherical counterparts in a manner that involves GpsB.

There are several other lines of evidence that give additional credence to the GpsB-WTA link. The first comes from the suppressor analysis in *L. monocytogenes* (42), where Rismondo et al. show that suppressor mutations in the WTA biosynthesis pathway can suppress the lethality of cells growing without *gpsB* at a higher nonpermissive temperature. These suppressors could be freeing lipid-II/UDP-GlcNAc for the essential peptidoglycan biosynthesis pathway. It may be possible that several lipid-II- and/or UDP-GlcNAc-utilizing WTA proteins and peptidoglycan synthesis components could be streamlined with the help of GpsB as a central coordinator for efficient cell cycle progression.

Another line of evidence supporting a GpsB-WTA link is the connection between WTA and division site localization/selection in multiple organisms. It has been shown that WTA machinery is enriched at the division site in both *B. subtilis* and *S. aureus* from the very start of septal membrane invagination (21, 23). Interestingly, PBP4, a likely interaction partner of GpsB (22), depends on TarO for division site localization (23). Investigations showed that inhibition of WTA synthesis (24, 43) or prevention of WTA transfer to peptidoglycan (44–46)

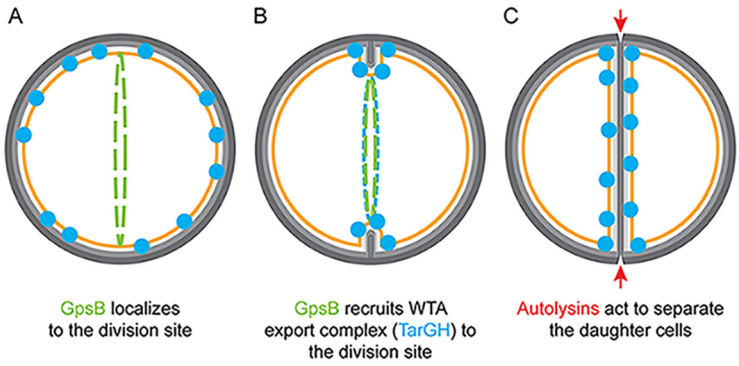

FIG 7 Model of GpsB-mediated coordination of cell division and wall teichoic acid export. (A) GpsB localizes to the division site in a FtsZ-dependent manner (15). (B) At the onset of membrane invagination, GpsB recruits WTA export machinery to the site of cell division. (C) Autolysins specifically act at the division septum to detach the daughter cells. GpsB, green; TarGH, blue; autolysins, red; membrane, orange; light and dark gray, less-cross-linked cell wall and WTA-rich highly cross-linked cell wall, respectively (24, 48, 49).

affects the positioning of division septum in *S. aureus*, which indicates a direct or indirect role for WTA in division site selection. Of note, at least one of the WTA ligases in *S. aureus*, SA1195 (MsrR), may interact with GpsB (22). Additionally, division site localization of the LTA synthesis complex in *S. aureus* has been noted previously (31), and it was shown that multiple proteins in the LTA machinery interact with the divisome, including PBPs and the well-characterized interaction partner of GpsB, EzrA. It is important to note that LTA synthesis happens extracellularly in the periplasmic space between the high-density cell wall zone and the membrane (47). WTA synthesis, on the other hand, occurs intracellularly and is exported for covalent attachment to the peptidoglycan to be part of the high-density cell wall zone (47). It is estimated that WTA makes up nearly 60% of the cell wall composition (19).

Evidence showing the presence of septal WTA is available (19, 24, 48, 49), and multiple studies have investigated the role and importance of WTA at sites of division. It has been proposed that the maturation (such as D-alanylation) and/or accumulation of WTA may then take place subsequent to cell division in order to not interfere with (or allow) the autolysin function (19, 23, 27, 50–53). In support of this idea, it was reported that LytF, a major autolysin in *B. subtilis*, is excluded from the lateral cell wall and localizes specifically to division sites in a WTA-dependent manner (33). Perhaps autolysins interact with WTAs to allow for efficient separation of conjoined daughter cells in one, or a combination, of the following three ways: autolysins are actively recruited to the division sites with the aid of immature WTAs (51), secretion of autolysins preferentially happen with WTA export at sites of division (28), and/or septum-localized proteins such as FmtA selectively remove D-alanylation at the division site (54). Additionally, other proteins that are translocated specifically at division sites, such as those with YSIRK signal, may rely on teichoic acids as well (55).

Taking the multiple lines of evidence into consideration, it is reasonable to postulate the presence of a multiprotein complex of complexes comprising the divisome (including septal peptidoglycan synthesis components) and machineries involved in synthesizing both WTA and LTA at the site of cell division. As such, we propose a model taking previously published reports into account (Fig. 7). GpsB initially localizes to the sites of cell division in an FtsZ-dependent manner (15). As shown in this study, TarG directly interacts with GpsB (Fig. 5A and Fig. S5B) and is preferentially enriched at the division site (Fig. S5D). Thus, we believe the TarGH WTA export complex and possibly TarO (based on its interaction with GpsB [22] and enrichment at division site [23]) are recruited to the division site by GpsB in *S. aureus*. Subsequent to the creation of the highly cross-linked WTA-containing cell wall at the septum (shown as dark gray lines in Fig. 7B and C) and secretion of autolysin at the division site, regulated autolysis allows for daughter cell separation, within the scale of milliseconds (30, 56). Immediately after cell separation, peripherally localized GpsB (15) may facilitate the continuous incorporation of WTA along the surface of the cell to further strengthen the cell envelope. Thus, we propose that GpsB aids in the coordination of cell division and WTA

synthesis/export machineries in *S. aureus*. Further investigation is necessary to shed light on the dependency of multiple crucial cellular processes on GpsB and the nature of molecular interaction between GpsB and its multiple partners. Given the significance of GpsB in multiple cellular pathways, it is an attractive drug target for the development of anti-staphylococcal/antibiotic compounds.

MATERIALS AND METHODS

Suppressor screen. Suppressor screening was carried out in the same manner as described previously (16). Strain GG8 (*gpsB^{SA}-gfp*) was plated onto LB agar plates supplemented with 1 mM IPTG to induce expression of *gpsB^{SA}-gfp* and incubated at 37°C overnight. Single colonies that were able to grow were then isolated from the plates and streaked onto new LB agar plates supplemented with 1 mM IPTG and incubated overnight at 37°C. After confirming the ability of these strains to grow, genomic DNA was extracted and transformed into fresh wild-type PY79 cells and screened for *amyE* integration. These colonies were then streaked onto LB agar plates supplemented with 1 mM IPTG, with PY79 serving as the control, and incubated overnight at 37°C. Strains that were not able to grow were denoted as possible extragenic mutations and sent for whole-genome sequencing (MiGS Microbial Genome Sequencing center, Pittsburgh, PA). In contrast, any strains that were able to grow in the presence of the IPTG inducer were denoted as possible **gpsB-gfp* intragenic suppressors. These strains were then screened via fluorescence microscopy to detect GFP signal and rule out possible promoter or frameshift mutations or the introduction of a premature stop codon. The genomic DNA from the **gpsB-gfp* strains was isolated, and the *amyE* locus carrying *gpsB-gfp* was PCR amplified (op36/op24) and subsequently sequenced. Analysis of the sequences was done using the ApE (A plasmid editor; M. Wayne Davis), and multiple sequence alignments were analyzed by using the Clustal Omega multiple sequence alignment software (57).

Strain construction. All relevant strain and oligonucleotide information is listed in Table S1. Construction of plasmids was performed with *E. coli* DH5α according to standard laboratory procedures. To generate *B. subtilis* strains carrying both mutated (labeled collectively as **gpsB-gfp*) and unmutated copies of *gpsB-gfp*, we utilized a PY79 (58) derivative that contains a second *amyE* locus (bkdB::Tn917::amyE::cat; Amy Camp). pGG4 (15) was used to clone *gpsB-gfp* into the second *amyE* locus making strain LH72. The resistance cassette was then switched from specR to ermR using pQP1 (Qi Pan) resulting in strain LH73. Following screening, genomic DNA from the **gpsB-gfp* strains was transformed into LH73 and colonies were screened for integration at the primary *amyE* locus. This process resulted in strains LH75-LH80 that have IPTG-inducible copies of both *gpsB-gfp* and **gpsB-gfp*. Initial generation of *B. subtilis* strains containing the **gpsB-gfp* mutations is described above (see "Suppressor screen"). *S. aureus* strains were constructed to place **gpsB-gfp* under the control of an IPTG-inducible promoter using the pCL15 plasmid backbone (59). The plasmid containing unmutated *gpsB-gfp*, pPE46 (15), was transformed into RN4220 cells resulting in strain GGS2. DNA for Y14F, D41G, D41G, ΔLEE, and R72H was PCR amplified (op36/oGG2; HindIII/SalI) and cloned into the pCL15 plasmid creating plasmids pLH5 to pLH9. L35S and LEErpt were made though QuikChange (Agilent) of pPE46 resulting in pPE78 and pPE80. These plasmids were then transformed into RN4220 cells, creating strains LH17 to 20 and LH35 to LH36. These plasmids were also transformed into the *S. aureus* RN4220 Δ*spa* background (SEJ1) (60) resulting in strains LH141 to LH159. The untagged ΔLEE strain was similarly created through PCR amplification (op36/op38 HindIII/SphI) and cloned into the pCL15 plasmid background creating pAH1 and transformed into RN4220 cells resulting in strain AH2. Plasmids for bacterial two-hybrid analysis were created using pEB354 and pEB355, which carry the pUT25 and pUT18 subunits of adenylate cyclase, respectively (17). DNA for *gpsB^{SA}* and **gpsB^{SA}* (BTH 11/BTH 12; EcoRI/XhoI; LH39-LH40, LH43-56), *tarG* (BTH62/BTH63; EcoRI/XhoI; SKB1-SKB2), and *tarH* (BTH 60/BTH61; EcoRI/XhoI; SKB3-SKB4) was PCR amplified and cloned into both pEB354 and pEB355. To create the *gfp-tagH* strain in *B. subtilis* cells, chromosomal DNA from Bacillus Genetic Stock Center (BGSC) 1A1119 (21) was transformed into PY79 cells to create PE528. Similarly, to create the CRISPRi TagG/TagH strains, chromosomal DNA was extracted from strains BEC35710 and BEC35700 (from BGSC), respectively, and transformed into PY79 cells to make SK15-SK16. Then, to create cells that contained the CRISPRi knockdown for TagG or TagH as well as IPTG-inducible *gpsB^{SA}-gfp*, the same DNA was transformed into LH72 resulting in SK17 to SK18. To create *gfp-tarG*, DNA was PCR amplified (oLH11/12; SalI/BamHI and oLH13/14; BamHI/EcoRI) and ligated into the pJB67 vector (61) resulting in pLH64, which was then transformed into RN4220 cells to make LH136. Finally, *gpsB^{SA}-flag* was created using two rounds of PCR to add the 3×FLAG tag onto the 3′ end of *S. aureus* GpsB (oP265 and oP302a/oP302b). The PCR product was the digested with BamHI and EcoRI and ligated into pJB67 to create pMR1. Following transformation into RN4220, the plasmid was transduced into SH1000 cells resulting in LH38.

Spot titer assay. The spot titer assays for *B. subtilis* strains were carried out on LB agar plates supplemented with 1 mM IPTG where needed to induce the expression of *gpsB^{SA}-gfp* or **gpsB^{SA}-gfp*. Cultures of the strains were first grown to mid-logarithmic phase (optical density at 600 nm [OD_{600}] of 0.4 to 0.6) and subsequently standardized to an OD_{600} of 0.1. The standardized cultures were then serially diluted and 1 μL of the liquid culture was spotted onto the appropriate plate. These plates were then incubated overnight at 37°C. Spot titer assays for *S. aureus* strains were completed in the same manner using tryptic soy agar plates supplemented with 10 μg/mL chloramphenicol and, where needed, 1 mM IPTG. The serial dilutions of the standardized cultures were spotted onto the plates with a volume of 1 μL. All experiments were conducted in triplicates and representative data are shown.

Fluorescence microscopy. Florescence microscopy was carried out as described previously (62). Overnight cultures of *B. subtilis* strains in LB liquid medium, or *S. aureus* strains in TSB supplemented with 10 μg/mL chloramphenicol (pCL15 backbone) or 5 μg/mL erythromycin (pJB67 backbone), were

diluted to OD_{600} of 0.1 and grown at 37°C to mid-logarithmic phase (OD_{600} of 0.4 to 0.6). Then, for *B. subtilis* cultures, where needed, 1 mM IPTG or 1% xylose was added to the cultures and grown for an additional 3 h. For *S. aureus*, 1 mM IPTG (pCL15) or 1.25 μM $CdCl_2$ (pJB67) was added to the cultures (except GFP-TarG where no inducer was added) and where needed, 20 μg/mL tunicamycin or 8 μg/mL targocil was also added. Cells were then grown for an additional 1 h. Following incubation, 1-mL aliquots were then pelleted and resuspended in 100 μL PBS and 1 μg/mL SynaptoRed fluorescent dye to allow for visualization of the cell membranes. A culture aliquot (5 μL) was then transferred to a glass bottom dish (Mattek) and covered with a 1% agarose pad. Samples were imaged on a DeltaVision Core microscope system (Applied Precision/GE Healthcare) equipped with a Photometrics CoolSnap HQ2 camera and an environmental chamber. Seventeen planes were acquired every 200 nm, and the data were deconvolved using SoftWorx software. Cell diameter was measured using ImageJ and analysis completed in GraphPad Prism 9.

Bacterial two-hybrid assay. Plasmids carrying our genes of interest were transformed into *E. coli* BTH101 cells and plated onto LB agar containing 100 μg/mL ampicillin and 50 μg/mL kanamycin and incubated at 30°C for 48 h. A positive-control strain was made by transforming PE87 and PE88 carrying pUT25-zip and pUT18-zip into the BTH101 cells. A negative control was made by transforming empty pEB354 and pEB355 into the cells. The resulting colonies harboring the pairs of plasmids of interest were then isolated and grown overnight in liquid LB medium at 30°C supplemented with 100 μg/mL ampicillin, 50 μg/mL kanamycin, and 0.5 mM IPTG. The following day, 2 μL of culture was spotted onto MacConkey plates (BD Biosciences) supplemented with 10 mg/mL maltose, 100 μg/mL ampicillin, 50 μg/mL kanamycin, and 0.5 mM IPTG. Plates were then incubated for 24 h to 48 h at 30°C. β-Galactosidase assays were completed in the 96-well plate reader as previously described with some modification (63). A mixture of 450 μL Z buffer, 120 μL o-nitrophenyl-β-D-galactopyranoside (ONPG; 4 mg/mL in Z buffer), 5.7 μL β-mercaptoethanol, 285 μL (polymyxin B 20 mg/mL), and 60 μL of culture for each strain tested was prepared. A total of 200 μL of each mixture was then transferred in triplicate to a 96-well plate. Readings were taken in a BioTek plate reader, and Miller units were calculated. Results were graphed using GraphPad Prism 9. All experiments were conducted in triplicates, and representative data are shown.

Immunoblotting. Cells were grown overnight and the next morning diluted to an OD_{600} of 0.1. At an OD_{600} of 0.4 to 0.6, IPTG was added to the appropriate cultures and then grown for an additional 1 h (*S. aureus* and *E. coli*) or 3 h (*B. subtilis*). Aliquots of cultures (1 mL) were then collected and pelleted. Cell lysis of *B. subtilis* cells was completed by using a protoplast buffer containing 0.5 M sucrose, 20 mM $MgCl_2$, 10 mM KH_2PO_4, and 0.1 mg/mL lysozyme. *S. aureus* cells (in RN4220 Δ*spa* background [60]) were resuspended in 500 μL PBS with 5 μL lysostaphin (1 mg/mL in 20 mM sodium acetate) and incubated for 30 min at 37°C. DNase A (1 μL of 1 U/μL) was then added and allowed to incubate for an additional 30 min. *E. coli* cell pellets were resuspended in a lysis buffer (20 mM HEPES, 50 mM KCl, 5 mM $MgCl_2$, 10% glycerol, 0.5 mg/ml lysozyme, and 1 mM PMSF) and incubated for 1 h at room temperature. Samples were then prepared for SDS-PAGE analysis. After electrophoresis, the samples were transferred to a membrane and probed with rabbit antisera raised against FLAG (Proteintech), GFP (K. Ramamurthi), and *B. subtilis* SigA (M. Fujita), or $GpsB^{SA}$-GFP, with total protein visualized using the GelCode Blue safe protein stain (ThermoFisher).

Coimmunoprecipitation assay. Coimmunoprecipitation (co-IP) assay was completed using the FLAG immunoprecipitation kit (Sigma). Overnight cultures of LH136 (GFP-TarG) and LH38 (GpsB-FLAG; functional fusion based on toxicity assay in *B. subtilis*) were standardized to an OD_{600} of 0.1 and grown to mid-log phase (OD_{600} = 0.4) and then induced using 1.25 μM $CdCl_2$ and allowed to grow for an additional hour. The 20-mL culture of LH136 was then formaldehyde cross-linked (60) with 1 mL of 16% methanol-free formaldehyde (Fisher). Following 20 min of room temperature shaking incubation, the reaction was quenched with 20 mL of 0.125 M glycine and incubated for an additional 10 min. Both strains were pelleted and resuspended in 500 μL phosphate-buffered saline (1× PBS). Sarkosyl (final concentration 0.5%) was added to LH136, and both strains were treated with lysostaphin (stock concentration 1 mg/mL in 20 mM sodium acetate; LH136, 100 μL; LH38, 10 μL) and then incubated for 30 min at 37°C. DNase (2 μL of 1 U/μL) was then added to both strains and incubated for an additional 30 min. Cell lysates were then pelleted and supernatants were combined. The co-IP of the supernatant was carried out per manufacturer protocol. Briefly, the combined cell lysates were incubated with the ANTI-FLAG M2-agarose affinity gel overnight at 4°C. The following day, the samples were washed 3 times and eluted using the 3×FLAG peptide. Samples were then incubated at 95°C for 20 min to reverse cross-linking, further processed for SDS-PAGE analysis, and analyzed by immunoblotting.

WTA extraction. WTAs were extracted and visualized as described previously (64). Briefly, cultures of PES5 and PES13 were grown overnight and back diluted to an OD_{600} of 0.1 the next day. Cultures were then grown to mid-log before 1 mM IPTG was added, and then the cultures were grown for an additional 3 h. Cells were standardized to the same OD (OD_{600} of 1) and then pelleted and washed in SDS buffer. Cells were then boiled for 1 h and subsequently extensively washed in SDS buffer. The cells were then subjected to proteinase K treatment, and following washes in sterile distilled water, the WTA was extracted with NaOH overnight. The following day, the tubes were centrifuged to separate the WTA from leftover debris. The supernatant was then run on a native PAGE gel and visualized with Alcian Blue (1:20 dilution of 1.25% stock solution in 2% acetic acid) followed by silver staining (ThermoFisher) following manufacturer protocols and imaged on the Bio-Rad Chemidoc MP Imaging System. This assay was conducted in triplicate, and representative data are shown.

Autolysis assay. Autolysis assays were carried out as described previously (28). Overnight cultures were back diluted to an OD_{600} of 0.1. Cultures were grown at 37°C to mid-log (OD_{600} of 0.4 to 0.6), and then 1 mM IPTG, and targocil when needed, was added (5 μg/mL). Cells were then grown for an additional hour. Cells were then pelleted, washed twice in cold H_2O, and standardized to an OD_{600} of 0.8. Cells were then spun and resuspended in 0.5 M Tris-HCl (pH 7.2) and 0.05% Triton X-100. OD_{600} was monitored in a 96-well plate reader for 10 h at 37°C. Results were graphed using GraphPad Prism 9.

Structural analysis and multiple sequence alignment. The 3-dimensional model for the N-terminal domain of $GpsB^{Sa}$ (residues 1 to 70) was generated with the SWISS-MODEL homology-model server (18).

GpsB suppressor mutants and simulated interactions with homologous PBP complexes were generated with PyMOL (Schrödinger, LLC). PDB coordinates for *S. pneumoniae*, *B. subtilis*, and *L. monocytogenes* GpsB in complex with their associated PBPs were retrieved from the PDB, with accession IDs 6GQN, 6GP7, and 6GPZ (14).

SUPPLEMENTAL MATERIAL

Supplemental material is available online only.

SUPPLEMENTAL FILE 1, PDF file, 3.2 MB.

ACKNOWLEDGMENTS

We thank our lab members for comments on the manuscript. This work was funded by the National Institutes of Health grants R35GM133617 (P.J.E.) and R21AI164775 (Y.C. and P.J.E.). A preprint of the manuscript was posted on bioRxiv (65).

The conception and design of the study were completed by L.R.H., C.S., and P.J.E., data acquisition was completed by L.R.H., S.J.K., M.D.S., A.H.-N., and C.S., analysis and/or interpretation of the data were completed by L.R.H., S.J.K., M.D.S., C.S., Y.C., and P.J.E., and writing of the manuscript was completed by L.R.H., M.D.S., Y.C., and P.J.E.

REFERENCES

1. Haeusser DP, Margolin W. 2016. Splitsville: structural and functional insights into the dynamic bacterial Z ring. Nat Rev Microbiol 14:305–319. https://doi.org/10.1038/nrmicro.2016.26.
2. Eswara PJ, Ramamurthi KS. 2017. Bacterial cell division: nonmodels poised to take the spotlight. Annu Rev Microbiol 71:393–411. https://doi.org/10.1146/annurev-micro-102215-095657.
3. Errington J, Wu LJ. 2017. Cell cycle machinery in Bacillus subtilis. Subcell Biochem 84:67–101. https://doi.org/10.1007/978-3-319-53047-5_3.
4. Egan AJF, Errington J, Vollmer W. 2020. Regulation of peptidoglycan synthesis and remodelling. Nat Rev Microbiol 18:446–460. https://doi.org/10.1038/s41579-020-0366-3.
5. Pinho MG, Kjos M, Veening JW. 2013. How to get (a)round: mechanisms controlling growth and division of coccoid bacteria. Nat Rev Microbiol 11:601–614. https://doi.org/10.1038/nrmicro3088.
6. Halbedel S, Lewis RJ. 2019. Structural basis for interaction of DivIVA/GpsB proteins with their ligands. Mol Microbiol 111:1404–1415. https://doi.org/10.1111/mmi.14244.
7. Hammond LR, White ML, Eswara PJ. 2019. ¸vIVA la DivIVA!. J Bacteriol 201. https://doi.org/10.1128/JB.00245-19.
8. Claessen D, Emmins R, Hamoen LW, Daniel RA, Errington J, Edwards DH. 2008. Control of the cell elongation-division cycle by shuttling of PBP1 protein in Bacillus subtilis. Mol Microbiol 68:1029–1046. https://doi.org/10.1111/j.1365-2958.2008.06210.x.
9. Tavares JR, de Souza RF, Meira GL, Gueiros-Filho FJ. 2008. Cytological characterization of YpsB, a novel component of the Bacillus subtilis divisome. J Bacteriol 190:7096–7107. https://doi.org/10.1128/JB.00064-08.
10. Rismondo J, Cleverley RM, Lane HV, Großhennig S, Steglich A, Möller L, Mannala GK, Hain T, Lewis RJ, Halbedel S. 2016. Structure of the bacterial cell division determinant GpsB and its interaction with penicillin-binding proteins. Mol Microbiol 99:978–998. https://doi.org/10.1111/mmi.13279.
11. Land AD, Tsui H-CT, Kocaoglu O, Vella SA, Shaw SL, Keen SK, Sham L-T, Carlson EE, Winkler ME. 2013. Requirement of essential Pbp2x and GpsB for septal ring closure in Streptococcus pneumoniae D39. Mol Microbiol 90:939–955. https://doi.org/10.1111/mmi.12408.
12. Fleurie A, Manuse S, Zhao C, Campo N, Cluzel C, Lavergne J-P, Freton C, Combet C, Guiral S, Soufi B, Macek B, Kuru E, VanNieuwenhze MS, Brun YV, Di Guilmi A-M, Claverys J-P, Galinier A, Grangeasse C. 2014. Interplay of the serine/threonine-kinase StkP and the paralogs DivIVA and GpsB in pneumococcal cell elongation and division. PLoS Genet 10:e1004275. https://doi.org/10.1371/journal.pgen.1004275.
13. Rued BE, Zheng JJ, Mura A, Tsui H-CT, Boersma MJ, Mazny JL, Corona F, Perez AJ, Fadda D, Doubravová L, Buriánková K, Branny P, Massidda O, Winkler ME. 2017. Suppression and synthetic-lethal genetic relationships of DeltagpsB mutations indicate that GpsB mediates protein phosphorylation and penicillin-binding protein interactions in Streptococcus pneumoniae D39. Mol Microbiol 103:931–957. https://doi.org/10.1111/mmi.13613.
14. Cleverley RM, Rutter ZJ, Rismondo J, Corona F, Tsui H-CT, Alatawi FA, Daniel RA, Halbedel S, Massidda O, Winkler ME, Lewis RJ. 2019. The cell cycle regulator GpsB functions as cytosolic adaptor for multiple cell wall enzymes. Nat Commun 10:261. https://doi.org/10.1038/s41467-018-08056-2.
15. Eswara PJ, Brzozowski RS, Viola MG, Graham G, Spanoudis C, Trebino C, Jha J, Aubee JI, Thompson KM, Camberg JL, Ramamurthi KS. 2018. An essential Staphylococcus aureus cell division protein directly regulates FtsZ dynamics. Elife 7. https://doi.org/10.7554/eLife.38856.
16. Brzozowski RS, Tomlinson BR, Sacco MD, Chen JJ, Ali AN, Chen Y, Shaw LN, Eswara PJ. 2020. Interdependent YpsA- and YfhS-mediated cell division and cell size phenotypes in Bacillus subtilis. mSphere 5. https://doi.org/10.1128/mSphere.00655-20.
17. Battesti A, Bouveret E. 2012. The bacterial two-hybrid system based on adenylate cyclase reconstitution in Escherichia coli. Methods 58:325–334. https://doi.org/10.1016/j.ymeth.2012.07.018.
18. Schwede T, Kopp J, Guex N, Peitsch MC. 2003. SWISS-MODEL: an automated protein homology-modeling server. Nucleic Acids Res 31:3381–3385. https://doi.org/10.1093/nar/gkg520.
19. Brown S, Santa Maria JP, Jr, Walker S. 2013. Wall teichoic acids of gram-positive bacteria. Annu Rev Microbiol 67:313–336. https://doi.org/10.1146/annurev-micro-092412-155620.
20. Peters JM, Colavin A, Shi H, Czarny TL, Larson MH, Wong S, Hawkins JS, Lu CHS, Koo B-M, Marta E, Shiver AL, Whitehead EH, Weissman JS, Brown ED, Qi LS, Huang KC, Gross CA. 2016. A comprehensive, CRISPR-based functional analysis of essential genes in bacteria. Cell 165:1493–1506. https://doi.org/10.1016/j.cell.2016.05.003.
21. Formstone A, Carballido-Lopez R, Noirot P, Errington J, Scheffers DJ. 2008. Localization and interactions of teichoic acid synthetic enzymes in Bacillus subtilis. J Bacteriol 190:1812–1821. https://doi.org/10.1128/JB.01394-07.
22. Kent VL. 2013. Cell wall architecture and the role of wall teichoic acid in Staphylococcus aureus. White Rose eTheses Online, University of Sheffield, Sheffield, UK.
23. Atilano ML, Pereira PM, Yates J, Reed P, Veiga H, Pinho MG, Filipe SR. 2010. Teichoic acids are temporal and spatial regulators of peptidoglycan cross-linking in Staphylococcus aureus. Proc Natl Acad Sci U S A 107:18991–18996. https://doi.org/10.1073/pnas.1004304107.
24. Campbell J, Singh AK, Santa Maria JP, Kim Y, Brown S, Swoboda JG, Mylonakis E, Wilkinson BJ, Walker S. 2011. Synthetic lethal compound combinations reveal a fundamental connection between wall teichoic acid and peptidoglycan biosyntheses in Staphylococcus aureus. ACS Chem Biol 6:106–116. https://doi.org/10.1021/cb100269f.
25. Campbell J, Singh AK, Swoboda JG, Gilmore MS, Wilkinson BJ, Walker S. 2012. An antibiotic that inhibits a late step in wall teichoic acid biosynthesis induces the cell wall stress stimulon in Staphylococcus aureus. Antimicrob Agents Chemother 56:1810–1820. https://doi.org/10.1128/AAC.05938-11.
26. Biswas R, Martinez RE, Göhring N, Schlag M, Josten M, Xia G, Hegler F, Gekeler C, Gleske A-K, Götz F, Sahl H-G, Kappler A, Peschel A. 2012. Proton-binding capacity of Staphylococcus aureus wall teichoic acid and its role in controlling autolysin activity. PLoS One 7:e41415. https://doi.org/10.1371/journal.pone.0041415.
27. Schlag M, Biswas R, Krismer B, Kohler T, Zoll S, Yu W, Schwarz H, Peschel A, Götz F. 2010. Role of staphylococcal wall teichoic acid in targeting the major autolysin Atl. Mol Microbiol 75:864–873. https://doi.org/10.1111/j.1365-2958.2009.07007.x.

28. Tiwari KB, Gatto C, Walker S, Wilkinson BJ. 2018. Exposure of Staphylococcus aureus to targocil blocks translocation of the major autolysin Atl across the membrane, resulting in a significant decrease in autolysis. Antimicrob Agents Chemother 62. https://doi.org/10.1128/AAC.00323-18.
29. Steele VR, Bottomley AL, Garcia-Lara J, Kasturiarachchi J, Foster SJ. 2011. Multiple essential roles for EzrA in cell division of Staphylococcus aureus. Mol Microbiol 80:542–555. https://doi.org/10.1111/j.1365-2958.2011.07591.x.
30. Monteiro JM, Fernandes PB, Vaz F, Pereira AR, Tavares AC, Ferreira MT, Pereira PM, Veiga H, Kuru E, VanNieuwenhze MS, Brun YV, Filipe SR, Pinho MG. 2015. Cell shape dynamics during the staphylococcal cell cycle. Nat Commun 6:8055. https://doi.org/10.1038/ncomms9055.
31. Reichmann NT, Piçarra Cassona C, Monteiro JM, Bottomley AL, Corrigan RM, Foster SJ, Pinho MG, Gründling A. 2014. Differential localization of LTA synthesis proteins and their interaction with the cell division machinery in Staphylococcus aureus. Mol Microbiol 92:273–286. https://doi.org/10.1111/mmi.12551.
32. Schirner K, Marles-Wright J, Lewis RJ, Errington J. 2009. Distinct and essential morphogenic functions for wall- and lipo-teichoic acids in Bacillus subtilis. EMBO J 28:830–842. https://doi.org/10.1038/emboj.2009.25.
33. Yamamoto H, Miyake Y, Hisaoka M, Kurosawa S, Sekiguchi J. 2008. The major and minor wall teichoic acids prevent the sidewall localization of vegetative DL-endopeptidase LytF in Bacillus subtilis. Mol Microbiol 70:297–310. https://doi.org/10.1111/j.1365-2958.2008.06397.x.
34. Kawai Y, Marles-Wright J, Cleverley RM, Emmins R, Ishikawa S, Kuwano M, Heinz N, Bui NK, Hoyland CN, Ogasawara N, Lewis RJ, Vollmer W, Daniel RA, Errington J. 2011. A widespread family of bacterial cell wall assembly proteins. EMBO J 30:4931–4941. https://doi.org/10.1038/emboj.2011.358.
35. Dominguez-Cuevas P, Porcelli I, Daniel RA, Errington J. 2013. Differentiated roles for MreB-actin isologues and autolytic enzymes in Bacillus subtilis morphogenesis. Mol Microbiol 89:1084–1098. https://doi.org/10.1111/mmi.12335.
36. Meisner J, Montero Llopis P, Sham LT, Garner E, Bernhardt TG, Rudner DZ. 2013. FtsEX is required for CwlO peptidoglycan hydrolase activity during cell wall elongation in Bacillus subtilis. Mol Microbiol 89:1069–1083. https://doi.org/10.1111/mmi.12330.
37. Sham LT, Barendt SM, Kopecky KE, Winkler ME. 2011. Essential PcsB putative peptidoglycan hydrolase interacts with the essential FtsXSpn cell division protein in Streptococcus pneumoniae D39. Proc Natl Acad Sci U S A 108:E1061–E1069. https://doi.org/10.1073/pnas.1108323108.
38. Du S, Henke W, Pichoff S, Lutkenhaus J. 2019. How FtsEX localizes to the Z ring and interacts with FtsA to regulate cell division. Mol Microbiol 112:881–895. https://doi.org/10.1111/mmi.14324.
39. Pichoff S, Du S, Lutkenhaus J. 2019. Roles of FtsEX in cell division. Res Microbiol 170:374–380. https://doi.org/10.1016/j.resmic.2019.07.003.
40. Tavares AC, Fernandes PB, Carballido-Lopez R, Pinho MG. 2015. MreC and MreD proteins are not required for growth of Staphylococcus aureus. PLoS One 10:e0140523. https://doi.org/10.1371/journal.pone.0140523.
41. Do T, Schaefer K, Santiago AG, Coe KA, Fernandes PB, Kahne D, Pinho MG, Walker S. 2020. Staphylococcus aureus cell growth and division are regulated by an amidase that trims peptides from uncrosslinked peptidoglycan. Nat Microbiol 5:291–303. https://doi.org/10.1038/s41564-019-0632-1.
42. Rismondo J, Bender JK, Halbedel S. 2017. Suppressor mutations linking gpsB with the first committed step of peptidoglycan biosynthesis in Listeria monocytogenes. J Bacteriol 199. https://doi.org/10.1128/JB.00393-16.
43. Santa Maria JP, Sadaka A, Moussa SH, Brown S, Zhang YJ, Rubin EJ, Gilmore MS, Walker S. 2014. Compound-gene interaction mapping reveals distinct roles for Staphylococcus aureus teichoic acids. Proc Natl Acad Sci U S A 111:12510–12515. https://doi.org/10.1073/pnas.1404099111.
44. Over B, Heusser R, McCallum N, Schulthess B, Kupferschmied P, Gaiani JM, Sifri CD, Berger-Bächi B, Stutzmann Meier P. 2011. LytR-CpsA-Psr proteins in Staphylococcus aureus display partial functional redundancy and the deletion of all three severely impairs septum placement and cell separation. FEMS Microbiol Lett 320:142–151. https://doi.org/10.1111/j.1574-6968.2011.02303.x.
45. Chan YG, Frankel MB, Dengler V, Schneewind O, Missiakas D. 2013. Staphylococcus aureus mutants lacking the LytR-CpsA-Psr family of enzymes release cell wall teichoic acids into the extracellular medium. J Bacteriol 195:4650–4659. https://doi.org/10.1128/JB.00544-13.
46. Li FKK, Rosell FI, Gale RT, Simorre JP, Brown ED, Strynadka NCJ. 2020. Crystallographic analysis of Staphylococcus aureus LcpA, the primary wall teichoic acid ligase. J Biol Chem 295:2629–2639. https://doi.org/10.1074/jbc.RA119.011469.
47. Reichmann NT, Grundling A. 2011. Location, synthesis and function of glycolipids and polyglycerolphosphate lipoteichoic acid in Gram-positive bacteria of the phylum Firmicutes. FEMS Microbiol Lett 319:97–105. https://doi.org/10.1111/j.1574-6968.2011.02260.x.
48. Matias VR, Beveridge TJ. 2007. Cryo-electron microscopy of cell division in Staphylococcus aureus reveals a mid-zone between nascent cross walls. Mol Microbiol 64:195–206. https://doi.org/10.1111/j.1365-2958.2007.05634.x.
49. Matias VR, Beveridge TJ. 2006. Native cell wall organization shown by cryo-electron microscopy confirms the existence of a periplasmic space in Staphylococcus aureus. J Bacteriol 188:1011–1021. https://doi.org/10.1128/JB.188.3.1011-1021.2006.
50. Nega M, Tribelli PM, Hipp K, Stahl M, Gotz F. 2020. New insights in the coordinated amidase and glucosaminidase activity of the major autolysin (Atl) in Staphylococcus aureus. Commun Biol 3:695. https://doi.org/10.1038/s42003-020-01405-2.
51. Bonnet J, Durmort C, Mortier-Barrière I, Campo N, Jacq M, Moriscot C, Straume D, Berg KH, Håvarstein L, Wong Y-S, Vernet T, Di Guilmi AM. 2018. Nascent teichoic acids insertion into the cell wall directs the localization and activity of the major pneumococcal autolysin LytA. Cell Surf 2:24–37. https://doi.org/10.1016/j.tcsw.2018.05.001.
52. Frankel MB, Schneewind O. 2012. Determinants of murein hydrolase targeting to cross-wall of Staphylococcus aureus peptidoglycan. J Biol Chem 287:10460–10471. https://doi.org/10.1074/jbc.M111.336404.
53. Qamar A, Golemi-Kotra D. 2012. Dual roles of FmtA in Staphylococcus aureus cell wall biosynthesis and autolysis. Antimicrob Agents Chemother 56:3797–3805. https://doi.org/10.1128/AAC.00187-12.
54. Rahman MM, Hunter HN, Prova S, Verma V, Qamar A, Golemi-Kotra D. 2016. The Staphylococcus aureus methicillin resistance factor FmtA is a d-amino esterase that acts on teichoic acids. mBio 7:e02070-15. https://doi.org/10.1128/mBio.02070-15.
55. Zhang R, Shebes MA, Kho K, Scaffidi SJ, Meredith TC, Yu W. 2021. Spatial regulation of protein A in Staphylococcus aureus. Mol Microbiol 116:589–605. https://doi.org/10.1111/mmi.14734.
56. Zhou X, Halladin DK, Rojas ER, Koslover EF, Lee TK, Huang KC, Theriot JA. 2015. Bacterial division. Mechanical crack propagation drives millisecond daughter cell separation in Staphylococcus aureus. Science 348:574–578. https://doi.org/10.1126/science.aaa1511.
57. Sievers F, Wilm A, Dineen D, Gibson TJ, Karplus K, Li W, Lopez R, McWilliam H, Remmert M, Söding J, Thompson JD, Higgins DG. 2011. Fast, scalable generation of high-quality protein multiple sequence alignments using Clustal Omega. Mol Syst Biol 7:539. https://doi.org/10.1038/msb.2011.75.
58. Youngman P, Perkins JB, Losick R. 1984. Construction of a cloning site near one end of Tn917 into which foreign DNA may be inserted without affecting transposition in Bacillus subtilis or expression of the transposon-borne erm gene. Plasmid 12:1–9. https://doi.org/10.1016/0147-619X(84)90061-1.
59. Luong TT, Lee CY. 2006. The arl locus positively regulates Staphylococcus aureus type 5 capsule via an mgrA-dependent pathway. Microbiology (Reading) 152:3123–3131. https://doi.org/10.1099/mic.0.29177-0.
60. Yu W, Missiakas D, Schneewind O. 2018. Septal secretion of protein A in Staphylococcus aureus requires SecA and lipoteichoic acid synthesis. Elife 7. https://doi.org/10.7554/eLife.34092.
61. Windham IH, Chaudhari SS, Bose JL, Thomas VC, Bayles KW. 2016. SrrAB modulates Staphylococcus aureus cell death through regulation of cidABC transcription. J Bacteriol 198:1114–1122. https://doi.org/10.1128/JB.00954-15.
62. Brzozowski RS, White ML, Eswara PJ. 2019. Live-cell fluorescence microscopy to investigate subcellular protein localization and cell morphology changes in bacteria. J Vis Exp https://doi.org/10.3791/59905.
63. Priest DG, Cui L, Kumar S, Dunlap DD, Dodd IB, Shearwin KE. 2014. Quantitation of the DNA tethering effect in long-range DNA looping in vivo and in vitro using the Lac and lambda repressors. Proc Natl Acad Sci U S A 111:349–354. https://doi.org/10.1073/pnas.1317817111.
64. Kho K, Meredith TC. 2018. Salt-induced stress stimulates a lipoteichoic acid-specific three-component glycosylation system in Staphylococcus aureus. J Bacteriol 200. https://doi.org/10.1128/JB.00017-18.
65. Hammond LR, Khan SJ, Sacco MD, Spanoudis C, Hough A, Chen Y, Eswara PJ. 2021. GpsB coordinates cell division and cell surface decoration by wall teichoic acids in Staphylococcus aureus. bioRxiv. https://doi.org/10.1101/2021.09.29.462461.